


Clostridium butyricum Alleviates Gut Microbiota Alteration–Induced Bone Loss after Bariatric Surgery by Promoting Bone Autophagy

Xueying Shang, Xiaolei Zhang, Cen Du, Zhuoqi Ma, Shi Jin, Na Ao, Jing Yang, and  Jian Du

Department of Endocrinology, The Fourth Affiliated Hospital of China Medical University, Shenyang, Liaoning, China

Received November 9, 2020; accepted March 1, 2021

ABSTRACT

Bariatric surgery is the most common and effective treatment of severe obesity; however, these bariatric procedures always result in detrimental effects on bone metabolism by underlying mechanisms. This study aims to investigate the skeletal response to bariatric surgery and to explore whether *Clostridium butyricum* alleviates gut microbiota alteration–induced bone loss after bariatric surgery. Consequently, male SD rats received Roux-en-Y gastric bypass (RYGB) and sleeve gastrectomy (SG) surgery, respectively, followed by body weight recording. The bone loss after bariatric surgery was further determined by dual-energy X-ray absorptiometry (DXA), micro-CT measurement, histologic analyses, and Western blot. Besides, 16S rDNA gene sequencing was performed to determine the gut microbiota alteration after surgery, and intervention with fecal microbiota from RYGB donor was conducted in obese SD rats, followed by *C. butyricum* administration. Accordingly, rats in the RYGB and SG groups maintained sustained weight loss, and DXA and micro-CT measurement further demonstrated significant bone loss after bariatric surgery. Besides, histologic and Western blot analyses validated enhanced osteoclastogenesis and inhibited

osteoblastogenesis and defective autophagy after surgery. The 16S rDNA gene sequencing suggested a significant alteration of gut microbiota composition in the RYGB group, and intervention with fecal microbiota from RYGB donor further determined that this kind of alteration contributed to the bone loss after RYGB. Meanwhile, *C. butyricum* might protect against this postoperative bone loss by promoting osteoblast autophagy. In summary, this study suggests novel mechanisms to clarify the skeletal response to bariatric surgery and provides a potential candidate for the treatment of bone disorder among bariatric patients.

SIGNIFICANCE STATEMENT

The significance of this study is the discovery of obvious bone loss and defective autophagy after bariatric surgery. Besides, it is revealed that gut microbiota alterations could be the reason for impaired bone mass after bariatric surgery. Furthermore, *Clostridium butyricum* could alleviate the gut microbiota alteration–induced bone loss after bariatric surgery by promoting osteoblast autophagy.

Introduction

Obesity has been a global epidemic with increasing prevalence in adults, adolescents, and even children (Pizzorno, 2016). Individuals with severe obesity often suffer from several health complications and even have a shorter life expectancy than people without obesity (Pucci and Batterham, 2019). Nowadays, bariatric surgeries such as sleeve gastrectomy (SG) and Roux-en-Y gastric bypass (RYGB) have

been regarded as the most effective treatment for people suffering from obesity (Rahman and Azagury, 2017). Specifically, RYGB directly regulates the gastrointestinal anatomy and nutrient flow (Pucci and Batterham, 2019), whereas SG mainly implicates the resection of gastric fundus (Bredella et al., 2017). Although both surgeries can result in weight loss, RYGB is reported to bring about greater body weight loss and a lower risk of diabetes in the future (Salminen et al., 2018). More importantly, it is documented that adverse outcome with significant bone loss will arise after RYGB or SG surgery despite the supplementation with calcium and vitamin D (Scibora et al., 2015; Pizzorno, 2016; Bredella et al., 2017). In particular, people having RYGB surgery have shown an obvious alteration in the content of bone turnover markers

This research was funded by the Basic Research Project of the Educational Department of Liaoning Province [Grant JC2019022].

No author has an actual or perceived conflict of interest with the contents of this article.

<https://doi.org/10.1124/jpet.120.000410>.

ABBREVIATIONS: ALP, alkaline phosphatase; BD, bone density; BV/TV, bone volume over total volume; CB, *C. butyricum*; CTX-I, carboxy-terminal opeptide of type I collagen; DXA, dual-energy X-ray absorptiometry; GAPDH, glyceraldehyde-3-phosphate dehydrogenase; LC3, Microtubule-associated protein 1 light chain 3; Micro-CT, micro computed tomography; OCN, osteocalcin; OPG, Osteoprotegerin; rDNA, ribosomal DNA; PCR, polymerase chain reaction; RYGB, Roux-en-Y gastric bypass; RYGB D, RYGB donor; RYGBS, RYGB sham; RANKL, receptor activator of nuclear factor (NF)- κ B-ligand; SCFA, short-chain fatty acid; SD, Sprague-Dawley; SG, sleeve gastrectomy; SGS, SG sham; Sham D, sham donor; SMI, structure model index; Tb.N, trabecular number; Tb.Sp, trabecular spacing; Tb.Th, trabecular thickness; TRAP, Tartrate-resistant acid phosphatase.

(Ivaska et al., 2017; Kim et al., 2020), which further validates the bone loss after bariatric surgery by bone remodeling mechanisms. However, the loss of bone mass in people having SG surgery is reported to be less compared with those in the RYGB group (Bredella et al., 2017).

Recently, growing evidence has shown that gut microbiota is closely related to the pathogenesis of several disorders, such as Alzheimer's and Parkinson's disease (Compare et al., 2016; Sun and Shen, 2018). More interestingly, gut microbiota is further reported to have a close connection to bone metabolism, and the earliest research has demonstrated that the overgrowth of gut microbiota might elevate the risk of generating osteoporosis (Chen et al., 2017). As for the potential mechanisms by which gut microbiota mediates bone metabolism, it is believed that the gut microbiome may induce the formation of bone via promoting the synthesis of insulin-like growth factor-1 or affecting the process of vitamin D metabolism (Pacifi, 2018). Besides, it is also documented that the gut microbiota might participate in the regulation of bone metabolism through the immune system (Chen et al., 2017). More importantly, bariatric surgery has been documented to significantly influence several compositions of gut microbiota (Shao et al., 2017); thus, we wonder whether this kind of gut microbiome alteration might contribute to the impaired bone metabolism after bariatric surgery (Yu, 2014).

Clostridium butyricum is a strict Gram positive anaerobic bacterium widely distributed in the gut of organisms, including human and animals. The nontoxicogenic strain of *C. butyricum* has been used as a probiotic to treat digestive system disease in Asia (Li et al., 2018a) by changing microbiota composition in the digestive tract. Recently, research further suggests the beneficial effect of *C. butyricum* on bone-related disease, and it has been proven that oral administration of ID-CBT5101 (tyndallized *C. butyricum*) can relieve the osteoarthritis symptoms in monosodium iodoacetate-treated rats by regulating the expressions of inflammatory cytokines and bone metabolism factors (Sim et al., 2018). Consequently, the purpose of this study is to investigate whether intestinal flora changes contribute to the bone loss after bariatric surgery and explore whether *C. butyricum* could alleviate the gut microbiota alteration-induced bone loss after bariatric surgery with specific mechanisms.

Materials and Methods

Ethical Statement. The experimental protocol was approved by the Animal Ethics Committee of China Medical University (approval code: 2019099) and followed the National Institutes of Health guide for the care and use of laboratory animals. All effort has been made to minimize the suffering of the animals.

Bariatric Surgical Protocol. Male SD rats (8 weeks old) were housed at a temperature of $25 \pm 1^\circ\text{C}$ and humidity of 44%–55%. All rats were allowed ad libitum access to water and food with a 12-hour light/dark cycle. Rats were anesthetized by 3% pentobarbital sodium after fasting overnight and were divided into four groups ($n = 6$ per group): SG sham (SGS), SG, RYGB sham (RYGBS), and RYGB. SG, RYGB, and their sham surgeries were conducted according to previously published research (Bruinsma et al., 2015; Kaufman et al., 2019; Ying et al., 2019). Afterward, body weight change of each group was monitored every week for 10 consecutive weeks. At the end of the experiment, rats were sacrificed and feces, serum, and limb bone tissue were collected from each group.

16S rDNA Gene Sequencing. The fecal samples from each group were collected and stored at -80°C . The DNA from different samples

was then extracted using the DNA extraction kit (D4015; Omega) according to the manufacturer's instructions. Basically, the V3-V4 region of 16S rDNA genes was amplified with the performance of polymerase chain reaction (PCR). The primers used for PCR were listed as follows: forward primer 341F: 5'-CCTACGGGNGGCWGCAG-3'; reverse primer 805R: 5'-GACTACHVGGGTATCTAATCC-3'.

The PCR product was then confirmed and purified for further sequencing. Accordingly, samples were sequenced on an Illumina NOvaSeq platform based on the manufacturer's recommendations, and the analyses on the 16S rDNA gene sequences were performed using the Quantitative Insights into Microbial Ecology to illustrate the α diversity and β diversity of gut microbiota. Briefly, the α diversity indicated the species complexity among one sample, whereas the β diversity analysis was applied to assess the differences among different samples in species complexity. Furthermore, the alterations of bacteria taxa from phylum to genus were identified in different groups of fecal sampling.

Fecal Microbiota Intervention and *C. butyricum* Administration. Male specific pathogen-free SD rats (4 weeks old) were adaptively fed for a week and randomly divided into three groups ($n = 6$ per group): sham donor (Sham D), RYGB donor (RYGB D), and RYGB D + *C. butyricum* (CB). The SG group was dismissed owing to the results of 16S rDNA sequencing. During experimental modeling, feces from sham and RYGB donor was administered to the pseudo germ-free obese rats (achieved by high-fat diet and antibiotic treatments) by colocolysis with the indicated amount of fecal suspension (1.6 ml/kg). Besides, dissolution of *Clostridium tyroformis* capsule in PBS was performed to prepare *C. butyricum*, and it was further administered to the RYGB D + CB group of rats by colocolysis at the concentration of 2.5×10^5 CFU/kg after RYGB fecal microbiota intervention. Afterward, body weight of each group was recorded once a week for 10 consecutive weeks, and sampling of serum and limb bone was collected for further study at the end of experiments.

ELISA. The content of carboxy-terminal opeptide of type I collagen (CTX-I) and osteocalcin (OCN) in serum was determined by ELISA according to the manufacturer's instructions (USCN Life Science, Wuhan, China).

Dual-Energy X-Ray Absorptiometry. Whole-body bone density (BD) was measured using dual-energy X-ray absorptiometry (DXA). In detail, measurement of BD was made with a dual-energy \times radio bone density analyzer (GE Healthcare, Waukesha, WI), and the testing of the quality control model was first conducted for blanking. Afterward, experimental rats were anesthetized with 3.0% pentobarbital sodium solution and then placed onto the machine for DXA scanning using the standard procedures based on the manufacturer's instructions. Each rat received DXA scans three times, and rats were repositioned by the same operator for each measurement. Moreover, BD was calculated as previously published (Hussain and Han, 2019).

micro-CT Measurement. The microstructure of trabecular bone was determined by micro-CT (Skyscan1174 X-Ray Microtomograph; Bruker, Belgium) as previously described (Luo et al., 2016). In particular, the trabecular bone region of tibia was first defined at about 1.5 mm away from the growth plate of proximal tibia and scanned by a micro-CT system with high resolution for 125 slices. Besides, scan resolution was set as 12 μm . Subsequently, the region of interest (ROI) was set and software in the micro-CT system, including CTreconstruction (N-Recon), and CT Analyzer (CT-AN), was used to measure the parameters of trabecular bone microstructure, including the bone volume over total volume (BV/TV), trabecular thickness (Tb.Th), trabecular number (Tb.N), trabecular spacing (Tb.Sp), and structure model index (SMI).

Hematoxylin and Eosin Staining. Bone tissue samples from the left lower limbs were fixed in 10% formalin for 24 hours followed by paraffin embedding. The fixed bone tissue was sectioned at a thickness of 5 μm . Sections were subsequently stained with hematoxylin (H8070; Solarbio, China) and eosin (A600190; Sangon biotech, Shanghai) after being deparaffinized and rehydrated. After dehydration in a graded series of ethanol and xylene, images of sections were

captured with a microscope at 200 \times magnification (BX53; OLYMPUS, Japan).

Alkaline Phosphatase Staining. Bone tissue samples from the left lower limbs were fixed and paraffin-embedded as described in the method of H&E staining. After slicing and dewaxing, alkaline phosphatase (ALP) staining was performed on sections using the ALP detection kit (DE0001; LEAGENE, Beijing) according to the manufacturer's instructions. The hematoxylin (H8070; Solarbio) staining was further conducted for 5 minutes, followed by image capture. In particular, images were obtained with a microscope at 200 \times magnification (BX53; OLYMPUS).

TRAP Staining. Sections were prepared as previously described (Luo et al., 2016). More specifically, they were fixed, paraffin-embedded, and sliced at a thickness of 5 μ m. After being deparaffinized and rehydrated, TRAP staining was further performed on sections in accordance with the manufacturer's instructions (387A-1KT; Sigma). Subsequently, sections were counterstained with hematoxylin (H8070; Solarbio) for another 3 minutes. Images were then captured with a microscope at 200 \times magnification (BX53; OLYMPUS), and TRAP-positive cells were defined as osteoclasts.

Immunohistochemical Staining. Sections were obtained as described in the *Hematoxylin and Eosin Staining* section and incubated with the 0.1 M citrate antigen retrieval solution for 10 minutes to get antigen restored. After additional rinsing in PBS, sections were subjected to incubation of 3% H₂O₂ (10011218; Sinopharm Chemical Reagent) at room temperature for 15 minutes. The incubation of normal goat serum (SL038; Solarbio) was further performed at room temperature for another 15 minutes to guarantee the specificity of staining. Subsequently, sections were treated with the primary antibodies against RANKL (D263508-0025; Sangon Biotech), OPG (D221075-0025; Sangon Biotech), and beclin 1 (A7353; Abclonal, Wuhan) at a dilution ratio of 1:50 at 4°C overnight. Next, sections were subjected to the treatment of horseradish peroxidase-conjugated secondary antibody (31460, 1:500; Thermo Fisher) for 1 hour at 37°C. The staining of 2,4-diaminobutyric acid (DAB) and hematoxylin was further performed, followed by image capture by microscope (BX53; OLYMPUS).

Sirius Red Staining. Sections were prepared as previously described. The Sirius Red staining was performed with the incubation of saturated Sirius Red picric acid (G1471; Solarbio) for 5 minutes followed by sealing. Images of the pathologic sections were captured using a microscope at 200 \times magnification (BX53; OLYMPUS), suggesting the changes in the content of bone collagen.

Western Blot Analysis. The extraction of total protein from bone tissue samples was performed using RIPA (radioimmune precipitation assay) lysis buffer containing PMSF (1 mM), followed by protein quantification. Equal amounts of protein samples were loaded on the sodium dodecyl sulfate polyacrylamide gel electrophoresis for separation and then transferred to a polyvinylidene fluoride (PVDF) membrane. The membrane was incubated with primary antibodies against LC3II/I (1:1000, A19665; Abclonal), p62 (1:1000, A19700; Abclonal), and beclin 1 (1:1000, A7353; Abclonal) at 4°C overnight after being blocked with 5% skim milk for 1 hour. The PVDF membrane was subsequently rinsed and then treated with the indicated secondary antibody for 1 hour at room temperature. Finally, the bands of indicated proteins were visualized by enhanced chemiluminescence substrate (PE0010; Solarbio), and their abundance was analyzed by Gel-Pro-Analyzer (Media Cybernetics, Bethesda, MD). Internal reference was GAPDH.

Statistical Analysis. The results were presented as means \pm S.D. and analyzed by GraphPad Prism. Student's *t* test was used to analyze the difference between just two groups. Comparisons between groups were made by using one-way ANOVA followed by Tukey's tests. Any value of *P* less than 0.05 was considered statistically significant.

Results

Effect of Bariatric Surgery on Body Weight. As shown in Fig. 1A, male SD rats received RYGB and SG surgery,

respectively, followed by body weight recording (Fig. 1B), and it was indicated that the baseline body weights of different groups were not significantly different before the surgery. Besides, it was found that body weight in each group gradually decreased in the first 3 weeks after operation and steadily elevated until 7 weeks; rats in the RYGB group experienced significant body weight loss from the 2nd week after surgery compared with the RYGBS group (RYGBS, 2nd week, 511.57 \pm 19.99 vs. RYGB, 2nd week, 418.92 \pm 11.47, *P* < 0.0001). Meanwhile, the difference between the SGS and SG groups became significant from the 4th week after surgery (SGS, 4th week, 532.02 \pm 41.97 vs. SG, 4th week, 478.3 \pm 31.8, *P* < 0.05). Furthermore, it was determined that both RYGB and SG surgery could result in sustained and significant body weight loss when compared with their sham group at the 10th week after surgery (RYGBS, 649.73 \pm 25.16 vs. RYGB, 502 \pm 16.13, *P* < 0.0001; SGS, 634 \pm 50.06 vs. SG, 554 \pm 35.56, *P* < 0.05). However, rats in the RYGB group achieved greater body weight loss than those in the SG group after the surgery (RYGB, 502 \pm 16.13 vs. SG, 554 \pm 35.56, *P* < 0.05).

Effect of Bariatric Surgery on Bone Turnover Markers. As shown in Table 1, the content of CTX-I and OCN was determined by ELISA. In particular, CTX-I is an important marker of bone resorption, whereas OCN is a marker of bone formation. It was indicated that CTX-I production was significantly elevated after RYGB or SG surgery. However, the OCN content was significantly reduced in the RYGB and SG groups of rats.

Effect of Bariatric Surgery on Bone Metabolism in Rats. Whole-body BD was analyzed using DXA. As shown in Fig. 2A, rats that received RYGB surgery showed significantly lower BD when compared with their sham group. The trabecular bone microstructure of tibia in each group was determined by micro-CT (Fig. 2B), and it proved that the RYGB and SG rats both showed a lower BV/TV and Tb.N and higher Tb.Sp than rats in their sham groups. Nevertheless, no significant difference was found in the alteration of Tb.Th. Besides, the SMI was determined to be significantly elevated in both RYGB and SG groups. Result of H&E staining further indicated the significant pathologic changes in the bone tissue of RYGB and SG rats (Fig. 2C). In addition, activities of osteoblast and osteoclast were measured by ALP and TRAP staining, respectively, and it was determined that the RYGB and SG groups showed significantly decreased area with ALP staining and remarkably increased area with TRAP staining when compared with their sham groups (Fig. 2, D and E). Analysis of Sirius Red staining indicated a significant decrease in bone collagen fiber content with less red staining, which further validated the impaired bone metabolism in rats after bariatric surgery (Fig. 2F). Furthermore, the expression levels of osteoclastogenesis-related protein RANKL and antiosteoclastogenic-related factor OPG were determined by immunohistochemical staining. It was indicated that significantly upregulated expression of RANKL and downregulated OPG abundance were found after the bariatric surgery (Fig. 2G).

Effect of Bariatric Surgery on Osteoblast Autophagy in Rats. The Western blot analyses (Fig. 3A) indicated a significant decrease in LC3II/I and beclin 1 expression after the bariatric surgery. However, the protein level of p62 was found to be significantly elevated in both RYGB and SG rats. We thus believed that bariatric surgery could result in the

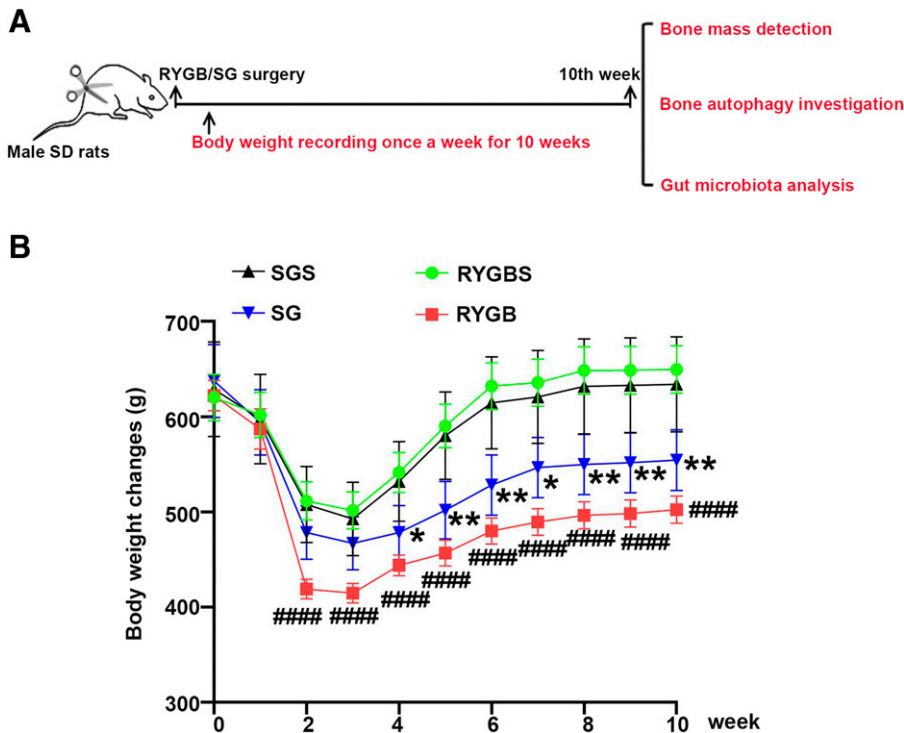


Fig. 1. Body weight alterations after bariatric surgery. (A) The experimental design is presented as a flowchart. SD rats were randomized to have RYGB or SG surgery, and body weight alterations were measured every week (B). Data are expressed as means \pm S.D. of $n = 6$. Compared with the RYGBS group: $^{\#}P < 0.05$; $^{\#\#}P < 0.01$; $^{\#\#\#}P < 0.001$; $^{\#\#\#\#}P < 0.0001$; compared with SGS group: $^*P < 0.05$; $^{**}P < 0.01$; $^{***}P < 0.001$; $^{****}P < 0.0001$.

defective bone autophagy in rats. It should be noted that osteoclast/osteoblast/osteocyte-mediated autophagy have all been implicated in the occurrence of bone loss, and they have specific distributions in bone tissue based on their functions. As a consequence, immunohistochemical staining of beclin 1 was further performed to identify the bone cell type that mediated autophagy in this study. As shown in Fig. 3, B and C, although positive staining of beclin 1 could be found in osteoblasts, osteoclasts, and osteocytes, beclin 1-positive osteoblasts were found to be significantly decreased in bone tissues of the RYGB/SG groups, which suggests that bariatric surgery could lead to defective osteoblast autophagy in rats.

Effect of Bariatric Surgery on Gut Microbiome in Rats. The 16S rDNA gene sequencing was performed to investigate the alteration in the gut microbiome of SD rats after bariatric surgery. Sequences with 97% similarity were assigned to the same operational taxonomic units by Vsearch. As shown in Fig. 4A, the shared and exclusive operational taxonomic units among samples were presented as a Venn diagram to suggest the similarities and overlaps between the gut microbiome of different groups. The Shannon index in Fig. 4B was analyzed to show the α diversity of gut microbiota. It was proven that the Shannon index was significantly reduced in the RYGB group when compared with its sham group, indicating that RYGB significantly reduces the species

diversity within samples. Besides, β diversity was further calculated by principal coordinate analysis (PCoA) of weighted UniFrac distance using Quantitative Insights Into Microbial Ecology (QIIME) software, and we found that there was an obvious distance between RYGB/SG and their sham groups (Fig. 4C), suggesting the reasonable grouping and sample credibility in this study. Furthermore, the microbial community structure of gut microbiota at phylum and genus levels was indicated as heatmap analysis according to their relative mean abundance (Fig. 4, D and F). It was revealed that the relative abundance of bacterial phyla and genus was differentially regulated in the RYGB group rather than SG when compared with their sham groups. More specifically, relative mean abundance of the top four bacterial phyla, Firmicutes, Bacteroidetes, Proteobacteria, and Verrucomicrobia, was separately analyzed (Fig. 4E). We found that the percentage of Firmicutes in the RYGB group was apparently lower than that in its sham group (RYGBS, 82.37 ± 4.31 vs. RYGB, 16.82 ± 10.37 , $P < 0.001$), whereas the proportions of Bacteroidetes, Proteobacteria, and Verrucomicrobia were found to be significantly higher than that in the RYGBS group ($P < 0.001$). At the genus level, the top eight bacterial genera were respectively assessed, and we found four of them (*Porphyromonadaceae unclassified*, *Bacteroides*, *Escherichia*, and *Akkermansia*) to be differentially upregulated and others (*Ruminococcaceae unclassified*, *Lachnospiraceae unclassified*,

TABLE 1

Effect of surgery on the bone turnover markers

All values are expressed as means \pm S.D. ($n = 6$).

Parameters	RYGBS	RYGB	SGS	SG
CTX-I (pg/ml)	1266 \pm 208	4385 \pm 96 $^{\#\#\#\#}$	1027 \pm 95	2836 \pm 276 ***
OCN (pg/ml)	2091.37 \pm 110.33	1256.92 \pm 100.65 $^{\#\#\#}$	1924.35 \pm 144.46	1008.33 \pm 126.73 **

$^{\#}P < 0.05$; $^{\#\#}P < 0.01$; $^{\#\#\#}P < 0.001$; $^{\#\#\#\#}P < 0.0001$, compared with RYGBS group. $^*P < 0.05$; $^{**}P < 0.01$; $^{***}P < 0.001$; $^{****}P < 0.0001$, compared with SGS group.

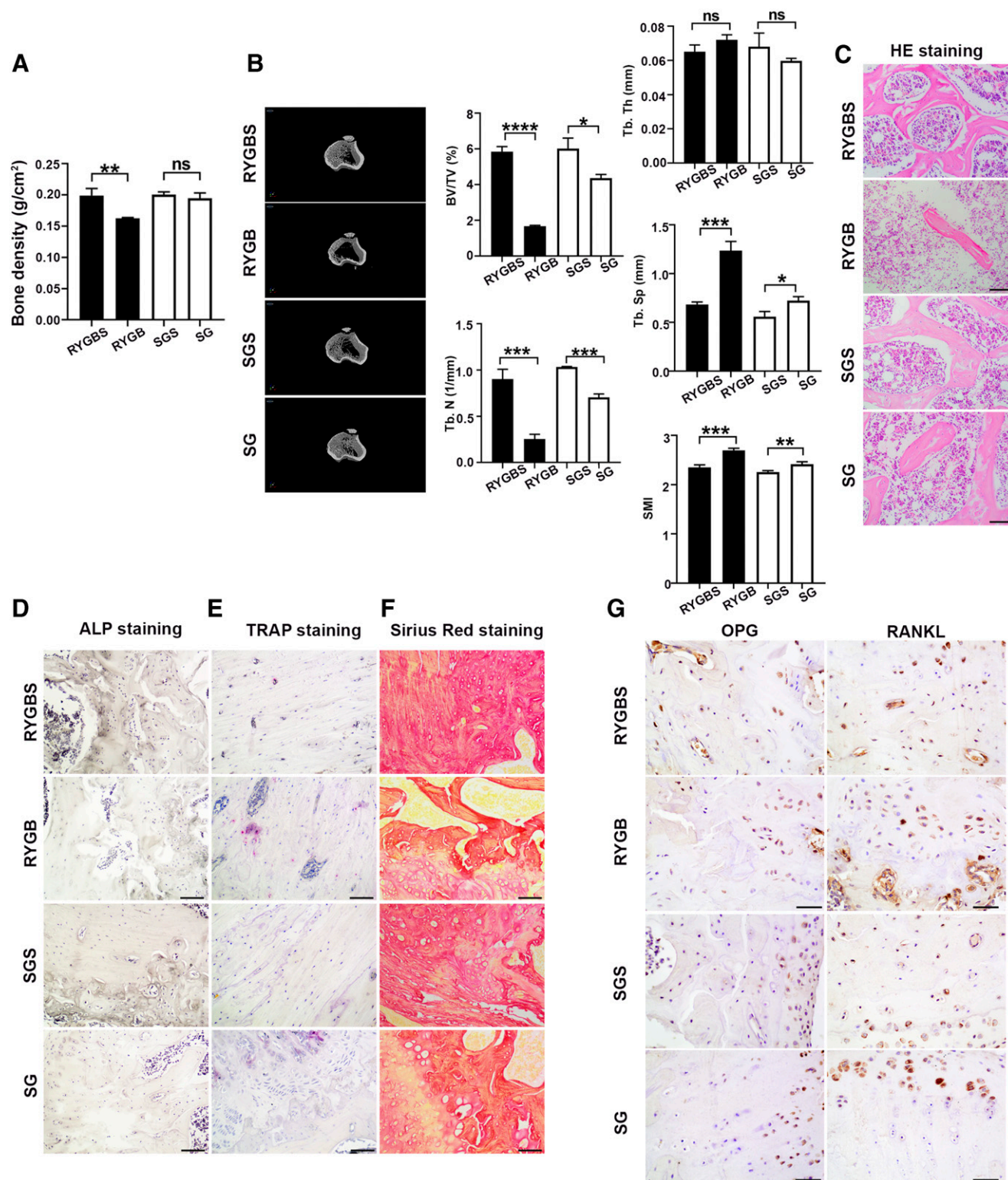


Fig. 2. Effect of bariatric surgery on bone metabolism in rats. (A) Whole-body bone density was determined by using DXA. (B) The trabecular bone microstructure of tibia in each group was determined by micro-CT with the analysis of BV/TV, Tb. Th, Tb. N, Tb.Sp, and SMI. (C) The pathologic alteration of each group was determined by H&E staining. Scale bar, 100 μ m. The activities of osteoblasts and osteoclasts in each group were respectively analyzed by ALP staining (D) and TRAP staining (E). Scale bar, 100 μ m. (F) The content of bone collagen of each group was assessed by Sirius Red staining. Scale bar, 100 μ m. (G) The expression levels of RANKL and OPG were detected by immunohistochemical staining. Scale bar, 50 μ m. Data are expressed as means \pm S.D. of $n = 6$. * $P < 0.05$; ** $P < 0.01$; *** $P < 0.001$; **** $P < 0.0001$.

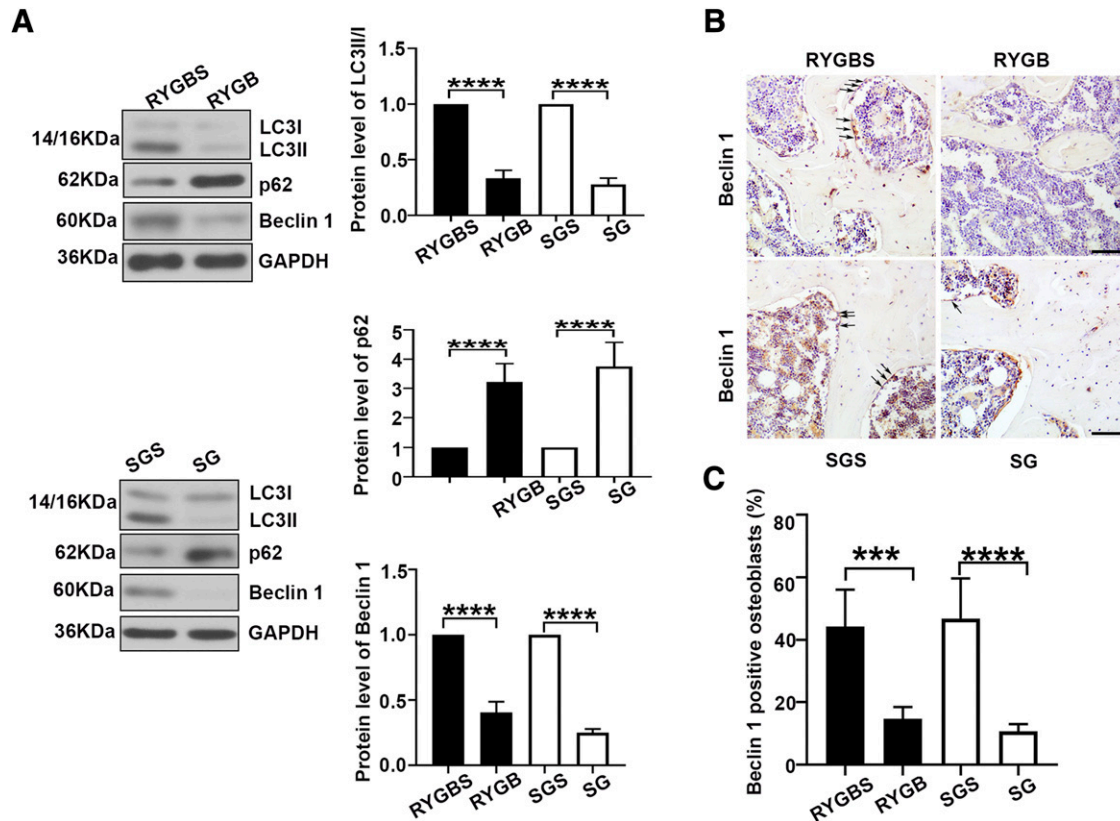


Fig. 3. Effect of bariatric surgery on osteoblast autophagy in rats. (A) The LC3II/I, p62, and beclin 1 expression levels were analyzed by Western blot. (B) The expression level of beclin 1 in each group was determined by immunohistochemical staining. Black arrow: beclin 1-positive osteoblasts. Scale bar, 100 μm. (C) Quantitative analysis of beclin 1-positive osteoblasts. Data are expressed as means \pm S.D. of $n = 6$. * $P < 0.05$; ** $P < 0.01$; *** $P < 0.001$; **** $P < 0.0001$.

Ruminococcus, and *Firmicutes unclassified*) to be downregulated (Fig. 4G) in the RYGB group.

Effect of *C. butyricum* and RYGB Fecal Microbiota Intervention on Body Weight in Pseudo Germ-Free Obese Rats. Considering the significant alteration of gut flora in the RYGB group compared with the SG group, RYGB fecal microbiota intervention was performed, followed by the *C. butyricum* administration on pseudo germ-free obese rats (Fig. 5A). Body weight change was recorded every week after the fecal microbiota intervention. Accordingly, rats in the RYGB D group showed a lower body weight from the 14th week, and *C. butyricum* intervention significantly protected against this kind of body weight loss from the 16th week (Fig. 5B).

Effect of RYGB Fecal Microbiota Intervention and *C. butyricum* Administration on Bone Turnover Markers. As shown in Table 2, CTX-I and OCN content was determined by ELISA. It was indicated that CTX-I production was significantly elevated after RYGB fecal microbiota intervention and reduced after *C. butyricum* administration. However, the OCN content was determined to be significantly reduced in the RYGB D group, whereas it was elevated after *C. butyricum* administration.

Effect of *C. butyricum* on RYGB Fecal Microbiota Intervention-Induced Impaired Bone Metabolism in Pseudo Germ-Free Obese Rats. The bone density after the RYGB fecal microbiota intervention was determined by DXA. It was indicated that rats in the RYGB D group possessed significantly reduced BD when compared with the sham group. Besides, BD was significantly elevated after the

C. butyricum administration (Fig. 6A). The microarchitectural bone parameters, including the BV/TV, Tb.Th, Tb.N, Tb.Sp, and SMI, were assessed using the in vitro micro-CT. As shown in Fig. 6B, rats in the RYGB D group showed a much lower BV/TV, Tb.N, and Tb.Th along with higher Tb.Sp when compared with sham group. The significantly elevated SMI further confirmed that the RYGB fecal microbiota intervention induced bone loss in obese rats. Moreover, treatment of *C. butyricum* was found to significantly reverse the effect on BV/TV, Tb.Th, and SMI, suggesting that *C. butyricum* might protect against the bone loss in RYGB D rats. H&E staining was performed to detect the pathologic alteration in bone tissues after the RYGB fecal microbiota intervention, and we determined that *C. butyricum* could significantly alleviate the pathologic changes in the RYGB D group (Fig. 6C). Reduced osteoblast activity and elevated osteoclast activity were found after the RYGB fecal microbiota intervention according to the ALP and TRAP staining (Fig. 6, D and E), and administration of *C. butyricum* significantly compensated for this effect. The Sirius Red staining in Fig. 6F suggested a loss of bone collagen content after the RYGB fecal microbiota intervention, and *C. butyricum* treatment significantly increased the collagen content. The osteoclastogenesis-related protein RANKL and antiosteoclastogenic factor OPG were further analyzed by immunohistochemical staining. Results in Fig. 6G indicated a significant augmentation in RANKL expression and attenuation in OPG expression after the RYGB fecal microbiota intervention. However, *C. butyricum* treatment displayed an inverse effect on these alterations.

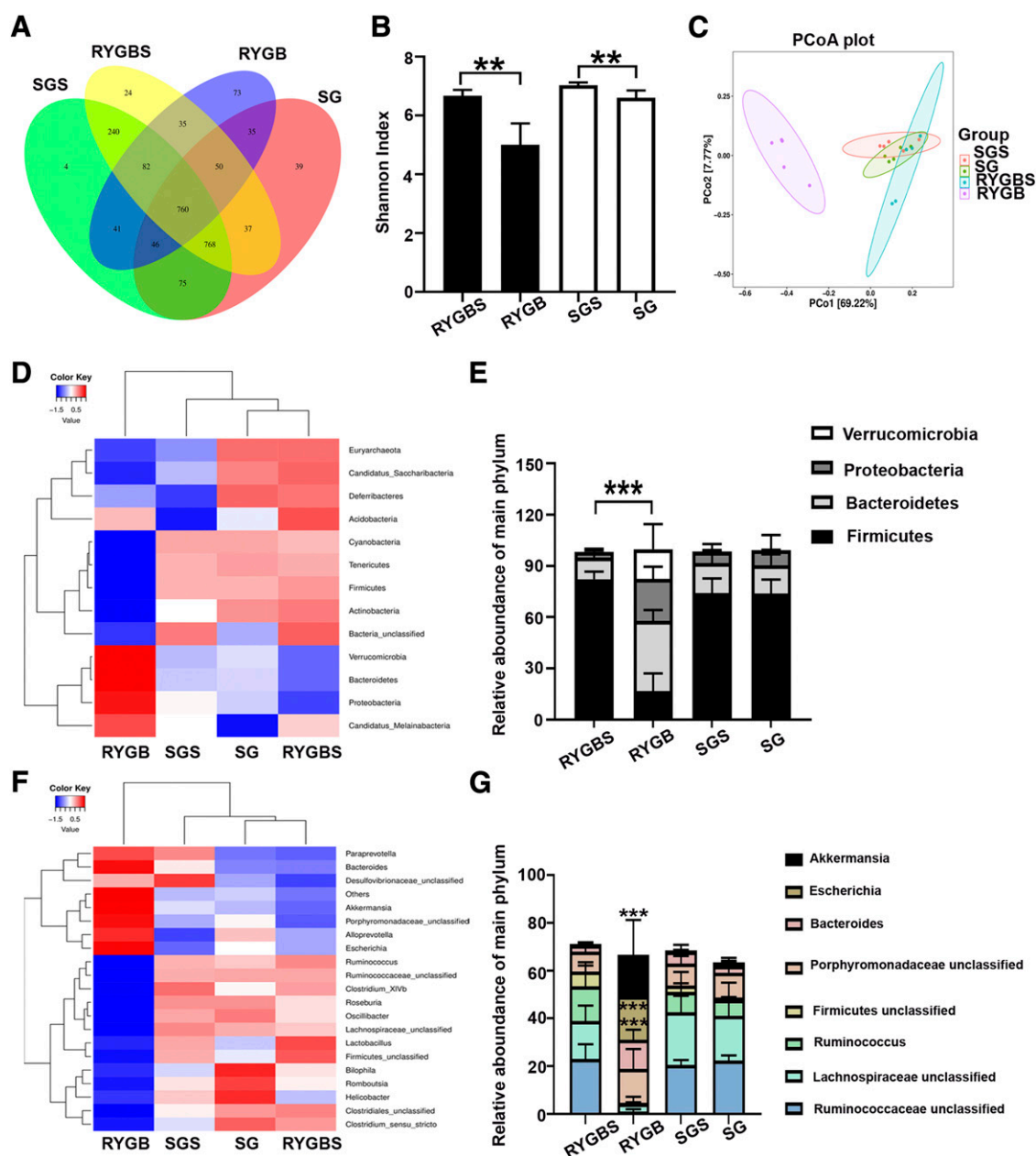


Fig. 4. Alterations of the gut microbiome after bariatric surgery. (A) The Venn diagram shows the similarities and overlap between four groups. (B) The Shannon index suggests α diversity among different groups. (C) The weighted PCoA plot analysis indicates the β diversity in each group. (D) The difference between different phyla is presented by heatmap. (E) Relative abundance analysis of top four bacterial phyla. (F) The genus-level differences in different groups is presented by heatmap. (G) Relative abundance analysis of the top eight differentiated bacterial genera. Data are expressed as means \pm S.D. of $n = 5$. * $P < 0.05$; ** $P < 0.01$; *** $P < 0.001$; **** $P < 0.0001$.

Effect of *C. butyricum* on RYGB Fecal Microbiota Intervention-Induced Osteoblast Autophagy in Pseudo Germ-Free Obese Rats. The Western blot analysis in Fig. 7, A–C determined the downregulated protein levels of LC3II/I and beclin 1 as well as the upregulated p62 expression in bone tissue after the RYGB fecal microbiota intervention, which suggested the defective bone autophagy. Moreover, *C. butyricum* treatment could promote the autophagy with the reversal of these changes. In line with Fig. 3B, immunohistochemical staining of beclin 1 was further performed to identify the bone cell type that mediated autophagy in this study. As shown in Fig. 7, D and E, although positive staining of beclin 1 could be found in osteoblasts, osteoclasts, and

osteocytes, beclin 1-positive osteoblasts were found to be significantly decreased in bone tissues in the RYGB D group and increased after *C. butyricum* treatment, which suggests that *C. butyricum* might alleviate the gut microbiota alteration-induced bone loss after bariatric surgery by promoting osteoblast autophagy.

Discussion

It has been suggested that increased skeletal fragility and higher risk of fracture are closely related to bariatric surgery (Nakamura et al., 2014), and prospective studies have indicated that significant bone loss is always accompanied by

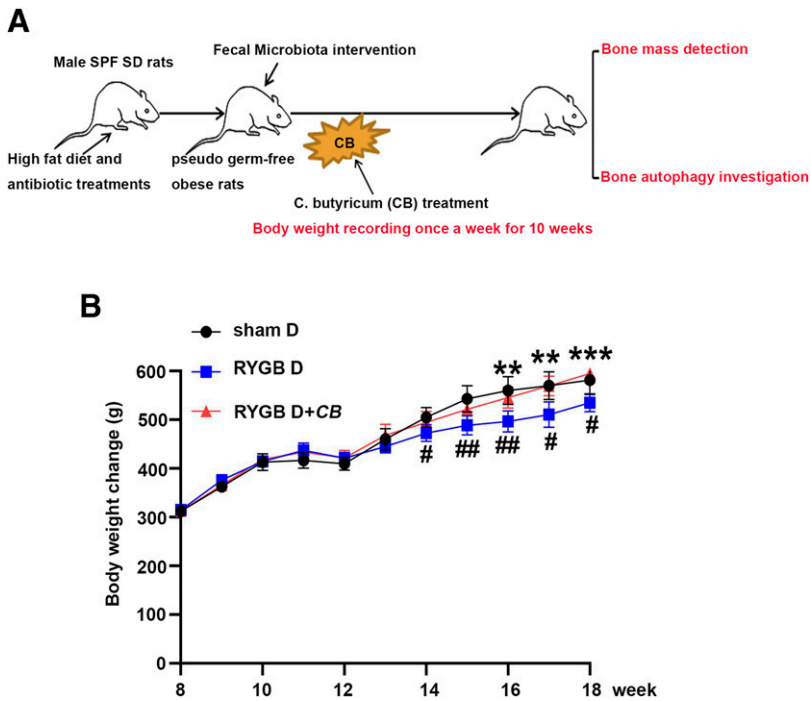


Fig. 5. Body weight alterations after the RYGB fecal microbiota transplantation and *C. butyricum* intervention. (A) The experimental design is presented as a flowchart. Obese rats received RYGB fecal microbiota transplantation and *C. butyricum* intervention. The body weight changes were recorded every week after manipulation (B). Data are expressed as means \pm S.D. of $n = 6$. Compared with the sham D group: $^{\#}P < 0.05$; $^{##}P < 0.01$; $^{###}P < 0.001$; $^{####}P < 0.0001$; compared with RYGBD group: $^{*}P < 0.05$; $^{**}P < 0.01$; $^{***}P < 0.001$; $^{****}P < 0.0001$.

this kind of surgery-related weight loss, proving that bariatric surgery has a profound effect on bone outcomes (Scibora, 2014). In this study, it was determined that bariatric surgery could cause significant bone loss based on the DXA and micro-CT analysis. Moreover, the acceleration of TRAP/CTX-I-mediated bone resorption and the impaired ALP/OCN-mediated bone formation was also found after the bariatric surgery, which confirms the defective bone metabolism after bariatric surgery. Actually, changes in bone metabolism after bariatric surgery are not surprising. It is reported that bariatric surgeries such as RYGB and SG both greatly reduce the intragastric volume, and the amount of food intake, and weaken the function of the digestive tract, which further accounts for the restricted absorption of vitamins and calcium that occurs afterward. Besides, it should be noted that alterations in vitamin and calcium absorption have shown essential effects on bone metabolism (Panda et al., 2004). More interestingly, this study further demonstrated the defective bone autophagy together with bone loss after bariatric surgery. Of note, osteoclast/osteoblast/osteocyte-mediated autophagy all have been documented to participate in the occurrence of bone loss, and they have specific distributions in bone tissue based on their functions. Specifically, it is documented that osteoclasts are a group of multinuclear cells that are located at the interface of bone tissue to absorb bone and finally leave a single marrow cavity (Cappariello et al., 2014; Juan et al., 2018). Osteoblasts are always characterized

as being located on the periosteum as closely arranged mononuclear cells (Roeder et al., 2016; Juan et al., 2018). As for osteocytes, they mainly distribute within mineralized matrix with the most abundant cell population (Kalajzic et al., 2013). As a consequence, immunohistochemical staining of beclin 1 was further performed to identify the bone cell type that mediated autophagy in this study, and it was shown that osteoblasts are mainly responsible for this kind of disorder. Actually, it has been reported that rapamycin-induced autophagy could significantly relieve the severity of senile osteoporosis (Luo et al., 2016), which suggests the beneficial effect of promoted autophagy on abnormal bone loss. Moreover, osteoblast-mediated defective autophagy has also been determined to cause obvious bone loss and results in the impairment of bone homeostasis (Li et al., 2018b), which is consistent with our findings.

Although the cause of bone loss after bariatric surgery is multifactorial, it has been suggested that gut microbiome changes might be related to the bone loss after bariatric surgery (Stein and Silverberg, 2014; Ibáñez et al., 2019). Thus, 16S rDNA gene sequencing was further performed in this study, with significant alterations observed in the gut microbiome of the RYGB group when compared with its sham group. As we know, our gastrointestinal tract has the greatest numbers of microorganisms, which are tightly associated with regulation of human nutrition, metabolism, and immune system function. More importantly, bariatric surgery is a basic

TABLE 2

Effect of RYGB fecal microbiota intervention and *C. butyricum* administration on bone turnover markers

All values are expressed as means \pm S.D. ($n = 6$).

Tests	Sham D	RYGB D	RYGB D + C.B
CTX-I (pg/ml)	2250 \pm 83	5098 \pm 452 $^{####}$	2492 \pm 208 ****
OCN (pg/ml)	1405.41 \pm 78.75	1103.63 \pm 170.22 $^{\#}$	1686.99 \pm 84.20 **

$^{\#}P < 0.05$; $^{##}P < 0.01$; $^{###}P < 0.001$; $^{####}P < 0.0001$, compared with Sham D group. $^{*}P < 0.05$; $^{**}P < 0.01$; $^{***}P < 0.001$; $^{****}P < 0.0001$, compared with RYGB D group.

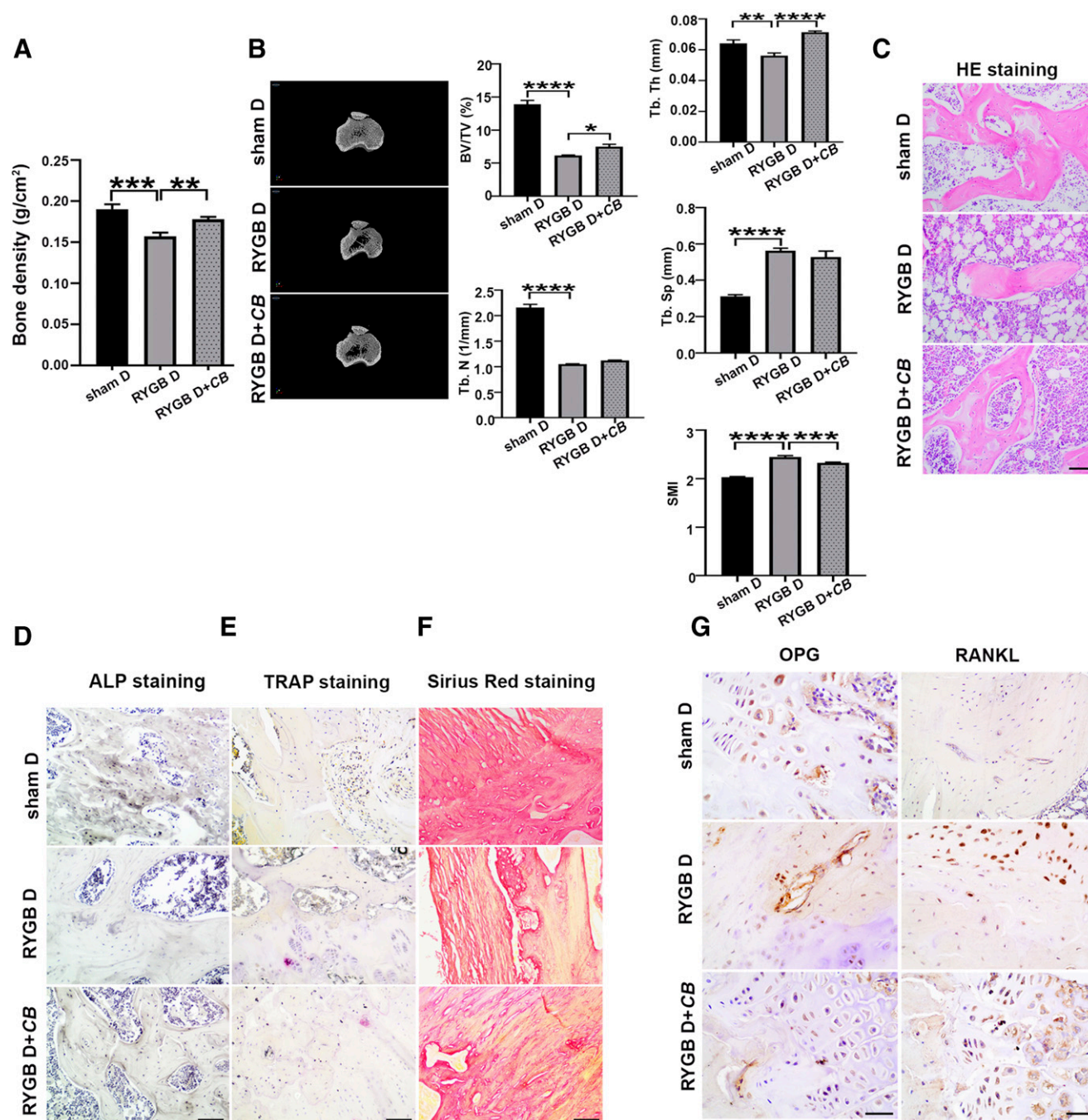


Fig. 6. Effect of *C. butyricum* on RYGB fecal microbiota transplantation-induced impaired bone metabolism in pseudo germ-free obese rats. (A) Whole-body bone density was determined by using DXA. (B) The images of tibia trabecular microstructure with micro-CT analyses in different groups. (C) The pathologic alterations in each group were determined by H&E staining. (D) The osteoblast activity was presented as ALP staining. Scale bar, 100 μ m. (E–F) TRAP and Sirius Red staining were respectively performed to analyze the activity of osteoclasts and collagen content. Scale bar, 100 μ m. (G) The expression levels of RANKL and OPG were determined by immunohistochemical staining. Scale bar, 50 μ m. Data are expressed as means \pm S.D. of $n = 6$. * $P < 0.05$; ** $P < 0.01$; *** $P < 0.001$; **** $P < 0.0001$.

method involving anatomic rearrangements in gastrointestinal tract, and this kind of alteration might further result in changes of the gut microbial community (Anhê et al., 2017). Besides, strong evidence has shown that the gut microbiome displays a profound effect on bone homeostasis (Pacifi, 2018). It is reported that microbiota is implicated in the regulation of bone growth and bone mass acquisition through multiple mechanisms. For example, it is documented that gut microbiota affects the absorption of calcium and phosphate by

influencing the fermentation of lactose and fructose (Daguet et al., 2016). Meanwhile, gut microbiota could promote the formation of bone via inducing the generation of a critical factor, insulin-like growth factor-1, to maintain bone health (Yan et al., 2016). Additionally, microbiota might affect the levels of vitamin D metabolites or steroid hormones to influence the bone cell function (Charles et al., 2015). In this study, a fecal microbiota intervention was conducted using the fecal samples from RYGB donors to investigate whether gut

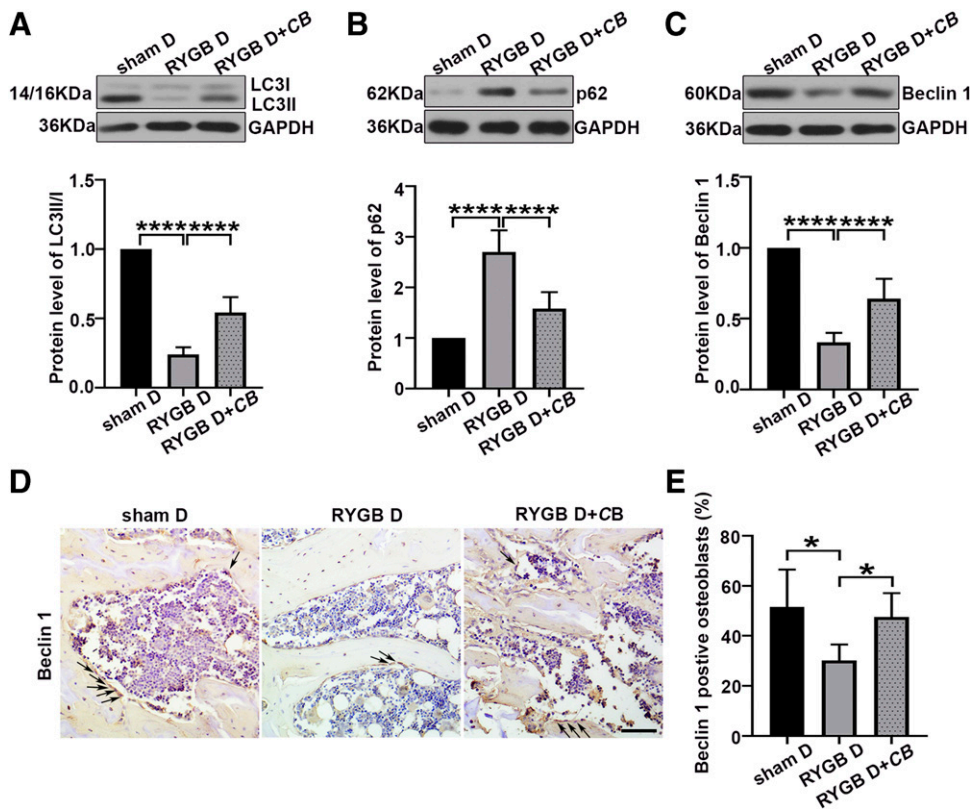


Fig. 7. Effect of *C. butyricum* on RYGB fecal microbiota transplantation-induced defective osteoblast autophagy in pseudo germ-free obese rats. (A–C) Western blot was conducted to measure the difference in protein levels of LC3II/I, p62, and beclin 1. (D) Immunohistochemical staining was performed to show the changes in beclin 1 expression. Black arrow: beclin 1-positive osteoblasts. Scale bar, 100 μ m. (E) Quantitative analysis of beclin 1-positive osteoblasts. Data are expressed as means \pm S.D. of $n = 6$. * $P < 0.05$; ** $P < 0.01$; *** $P < 0.001$; **** $P < 0.0001$.

microbiome changes contribute to the bone loss after bariatric surgery. According to the results of DXA and micro-CT measurements, it was discovered that the RYGB fecal microbiota intervention could result in significant bone loss in experimental rats when compared with their sham groups. Moreover, significantly upregulated osteoclast activity (termed TRAP staining) and downregulated osteoblast activity (termed ALP staining) were also determined in the RYGB D group of rats, suggesting the impairment of bone remodeling after fecal microbiota intervention. It is well established that bone is a dynamic tissue with two important processes, remodeling and modeling, which maintain bone homeostasis and regulate bone metabolism (Raggatt and Partridge, 2010). In particular, impairments of these two processes can cause diseases like osteoporosis. It should be noted that bone remodeling is mainly responsible for the removal and repair of destructive bones with the assistance of osteoblasts and osteoclasts (Kylmaja et al., 2016). Generally, it is tightly coordinated by the osteoclast-mediated bone resorption and the subsequent osteoblast-modulated bone formation. Osteoblasts are a group of bone-forming cells with several critical roles in bone remodeling, such as the regulation of osteoclastogenic factors, the generation of bone matrix proteins, and the mineralization of bone (Karsenty, 2008), whereas osteoclasts mainly contribute to bone resorption. More importantly, osteoblasts and osteoclasts could communicate with each other via indicated pathways. For instance, osteoblasts have been reported to affect formation, differentiation, and apoptosis of osteoclasts through OPG/RANKL/RANK signaling (Chen et al., 2018). Previous studies have indicated that RANKL could function as an activator of osteoclastogenesis, whereas OPG inhibits it (Bonnet et al., 2019). In accordance with this study, significantly elevated RANKL expression and

reduced OPG abundance were determined after RYGB fecal microbiota intervention, further validating the acceleration of osteoclastogenesis in the RYGB D group. In general, the present findings indicate that gut microbiota alteration accounts for bone loss after the bariatric surgery and enriches the mechanism of abnormal bone metabolism after the surgery.

Interestingly, the administration of *C. butyricum* after fecal microbiota intervention showed a significant protective effect on these bone abnormalities, suggesting the critical role of *C. butyricum* on bone metabolism. To the best of our knowledge, *C. butyricum* belongs to the family of Gram positive obligate anaerobic bacillus, and it is widely distributed in soil and animal and human intestines. The nontoxigenic strain of *C. butyricum* has been used as a probiotic in some Asian countries (Duncan et al., 2002), and it has also been proven to possess a strong ability to alleviate intestinal flora disorders by promoting the growth of probiotics such as *Bifidobacterium* and *Lactobacillus* (Hagihara et al., 2018). Accordingly, probiotic *Lactobacillus acidophilus* is documented to be able to inhibit the bone loss in osteoporotic mice by mediating the balance between regulatory T cell (Treg) and T helper cell 17 (Th17) (Dar et al., 2018). In addition, the beneficial effect of *Bifidobacterium* on bone metabolism has also been revealed in the model of experimental periodontitis via regulating the RANKL/OPG pathway (Oliveira et al., 2017). Moreover, *C. butyricum* has shown an important role in maintain the regular function of intestine epithelial barrier (Li et al., 2018a), which contributes a lot to the gut nutrition metabolism, especially the absorption of calcium and vitamin D, and further is implicated with regulation of bone health (Masuyama, 2014; Casselbrant et al., 2020). Besides, *C. butyricum* is also documented to display positive effects on bone metabolism

via regulating the gut microbiome and their metabolic short-chain fatty acids (SCFAs), such as acetate, propionate, and butyrate (Zaiss et al., 2019). Actually, SCFAs have a momentous role in the regulation of the musculoskeletal system, and some SCFAs are reported to regulate osteoclast differentiation and effectively prevent pathologic alterations in bone mass (Montalvany-Antonucci et al., 2019). More importantly, the promoted osteoblast autophagy was also observed after the *C. butyricum* intervention in the RYGB D group. A recent study has shown that osteoblast autophagy has been suggested as a potential therapeutic strategy against bone disorders, and it is documented that the enhanced autophagy of osteoblasts might alleviate remarkable bone loss by the mediation of sirtuin1 and phosphoinositide 3-kinase/protein kinase B/mammalian target of rapamycin signaling (Yang et al., 2019). However, the effect of *C. butyricum* on autophagy has not been extensively explored, which further suggests the novelty of this study.

In summary, this study indicates significant bone loss with defective autophagy after bariatric surgery. Besides, it is found that gut microbiota alterations could be one of the reasons for the impaired bone metabolism after bariatric surgery. Furthermore, *C. butyricum* alleviates the gut microbiota alteration-induced bone loss after bariatric surgery by promoting bone autophagy.

Authorship Contributions:

Participated in research design: Shang, J. Du.

Conducted experiments: Shang, Zhang, C. Du, Ma.

Performed data analysis: Jin, Ao, Yang.

Wrote or contributed to the writing of the manuscript: Shang, J. Du.

References

- Anhê FF, Varin TV, Schertzer JD, and Marette A (2017) The gut microbiota as a mediator of metabolic benefits after bariatric surgery. *Can J Diabetes* **41**:439–447.
- Bonnet N, Bourgoin L, Biver E, Douni E, and Ferrari S (2019) RANKL inhibition improves muscle strength and insulin sensitivity and restores bone mass. *J Clin Invest* **129**:3214–3223.
- Bredella MA, Greenblatt LB, Ejazi A, Torriani M, and Yu EW (2017) Effects of Roux-en-Y gastric bypass and sleeve gastrectomy on bone mineral density and marrow adipose tissue. *Bone* **95**:85–90.
- Bruinsma BG, Uygun K, Yarmush ML, and Saeidi N (2015) Surgical models of Roux-en-Y gastric bypass surgery and sleeve gastrectomy in rats and mice. *Nat Protoc* **10**:495–507.
- Cappariello A, Maurizi A, Verhaar V, and Teti A (2014) Reprint of: the great beauty of the osteoclast. *Arch Biochem Biophys* **561**:13–21.
- Casselbrant A, Fändriks L, and Wallenius V (2020) Glycocholic acid and butyrate synergistically increase vitamin D-induced calcium uptake in Caco-2 intestinal epithelial cell monolayers. *Bone Rep* **13**:100294.
- Charles JF, Ermann J, and Aliprantis AO (2015) The intestinal microbiome and skeletal fitness: connecting bugs and bones. *Clin Immunol* **159**:163–169.
- Chen X, Wang Z, Duan N, Zhu G, Schwarz EM, and Xie C (2018) Osteoblast-osteoclast interactions. *Connect Tissue Res* **59**:99–107.
- Chen Y-C, Greenbaum J, Shen H, and Deng H-W (2017) Association between gut microbiota and bone health: potential mechanisms and prospective. *J Clin Endocrinol Metab* **102**:3635–3646.
- Compare D, Rocco A, Sanduzzi Zamparelli M, and Nardone G (2016) The gut bacteria-driven obesity development. *Dig Dis* **34**:221–229.
- Daguet D, Pinheiro I, Verhelst A, Possemiers S, and Marzorati M (2016) Arabino-galactan and fructooligosaccharides improve the gut barrier function in distinct areas of the colon in the Simulator of the Human Intestinal Microbial Ecosystem. *J Funct Foods* **20**:369–379.
- Dar HY, Shukla P, Mishra PK, Anupam R, Mondal RK, Tomar GB, Sharma V, and Srivastava RK (2018) *Lactobacillus acidophilus* inhibits bone loss and increases bone heterogeneity in osteoporotic mice via modulating Treg-Th17 cell balance. *Bone Rep* **8**:46–56.
- Duncan SH, Hold GL, Barcenilla A, Stewart CS, and Flint HJ (2002) Roseburia intestinalis sp. nov., a novel saccharolytic, butyrate-producing bacterium from human faeces. *Int J Syst Evol Microbiol* **52**:1615–1620.
- Hagihara M, Yamashita R, Matsumoto A, Mori T, Kuroki Y, Kudo H, Oka K, Takahashi M, Nonogaki T, Yamagishi Y, et al. (2018) The impact of *Clostridium butyricum* MIYAIRI 588 on the murine gut microbiome and colonic tissue. *Anaerobe* **54**:8–18.
- Hussain D and Han SM (2019) Computer-aided osteoporosis detection from DXA imaging. *Comput Methods Programs Biomed* **173**:87–107.
- Ibáñez L, Rouleau M, Wakkach A, and Blin-Wakkach C (2019) Gut microbiome and bone. *Joint Bone Spine* **86**:43–47.
- Ivaska KK, Huovinen V, Soinio M, Hannukainen JC, Saunavaara V, Salminen P, Helmiö M, Parkkola R, Nuutila P, and Kiviranta R (2017) Changes in bone metabolism after bariatric surgery by gastric bypass or sleeve gastrectomy. *Bone* **95**:47–54.
- Juan L, Peng L, Mengjun W, and Yandong M (2018) Impact of hyperbaric oxygen on the healing of bone tissues around implants. *Implant Dent* **27**:653–659.
- Kalajzic I, Matthews BG, Torreggiani E, Harris MA, Divieti Pajevic P, and Harris SE (2013) In vitro and in vivo approaches to study osteocyte biology. *Bone* **54**:296–306.
- Karsenty G (2008) Transcriptional control of skeletogenesis. *Annu Rev Genomics Hum Genet* **9**:183–196.
- Kaufman S, Arnold M, Diaz AA, Neubauer H, Wolfrum S, Köfeler H, Langhans W, and Krieger J-P (2019) Roux-en-Y gastric bypass surgery reprograms enterocyte triglyceride metabolism and postprandial secretion in rats. *Mol Metab* **23**:51–59.
- Kim TY, Shoback DM, Black DM, Rogers SJ, Stewart L, Carter JT, Posselt AM, King NJ, and Schafer AL (2020) Increases in PYY and uncoupling of bone turnover are associated with loss of bone mass after gastric bypass surgery. *Bone* **131**:115115.
- Kylmaja E, Nakamura M, and Tuukkanen J (2016) Osteoclasts and remodeling based bone formation. *Curr Stem Cell Res Ther* **11**:626–633.
- Li H, Gong Y, Xie Y, Sun Q, and Li Y (2018a) *Clostridium butyricum* protects the epithelial barrier by maintaining tight junction protein expression and regulating microflora in a murine model of dextran sodium sulfate-induced colitis. *Scand J Gastroenterol* **53**:1031–1042.
- Li H, Li D, Ma Z, Qian Z, Kang X, Jin X, Li F, Wang X, Chen Q, Sun H, et al. (2018b) Defective autophagy in osteoblasts induces endoplasmic reticulum stress and causes remarkable bone loss. *Autophagy* **14**:1726–1741.
- Luo D, Ren H, Li T, Lian K, and Lin D (2016) Rapamycin reduces severity of senile osteoporosis by activating osteocyte autophagy. *Osteoporos Int* **27**:1093–1101.
- Masuyama R (2014) Role of local vitamin D signaling and cellular calcium transport system in bone homeostasis. *J Bone Miner Res* **32**:1–9.
- Montalvany-Antonucci CC, Duffles LF, de Arruda JAA, Zieker MC, de Oliveira S, Macari S, Garlet GP, Madeira MFM, Fukada SY, Andrade I Jr, et al. (2019) Short-chain fatty acids and FFAR2 as suppressors of bone resorption. *Bone* **125**:112–121.
- Nakamura KM, Haglund EGC, Clowes JA, Achenbach SJ, Atkinson EJ, Melton LJ III, and Kennel KA (2014) Fracture risk following bariatric surgery: a population-based study. *Osteoporos Int* **25**:151–158.
- Oliveira LF, Salvador SL, Silva PH, Furlaneto FA, Figueiredo L, Casarin R, Ervolino E, Paloto DB, Souza SL, Taba M Jr, et al. (2017) Benefits of *Bifidobacterium animalis* subsp. *lactis* probiotic in experimental periodontitis. *J Periodontol* **88**:197–208.
- Pacifici R (2018) Bone remodeling and the microbiome. *Cold Spring Harb Perspect Med* **8**:a031203.
- Panda DK, Miao D, Bolivar I, Li J, Huo R, Hendy GN, and Goltzman D (2004) Inactivation of the 25-hydroxyvitamin D 1alpha-hydroxylase and vitamin D receptor demonstrates independent and interdependent effects of calcium and vitamin D on skeletal and mineral homeostasis. *J Biol Chem* **279**:16754–16766.
- Pizzorno L (2016) Bariatric surgery: bad to the bone, Part 1. *Integr Med (Encinitas)* **15**:48–54.
- Pucci A and Batterham RL (2019) Mechanisms underlying the weight loss effects of RYGB and SG: similar, yet different. *J Endocrinol Invest* **42**:117–128.
- Raggatt LJ and Partridge NC (2010) Cellular and molecular mechanisms of bone remodeling. *J Biol Chem* **285**:25103–25108.
- Rahman R and Azagury DE (2017) Novel technologies and techniques in bariatric surgery. *Minerva Chir* **72**:125–139.
- Roeder E, Matthews BG, and Kalajzic I (2016) Visual reporters for study of the osteoblast lineage. *Bone* **92**:189–195.
- Salminen P, Helmiö M, Ovaska J, Juuti A, Leivonen M, Peromaa-Haavisto P, Hurme S, Soinio M, Nuutila P, and Victorzon M (2018) Effect of laparoscopic sleeve gastrectomy vs laparoscopic roux-en-Y gastric bypass on weight loss at 5 Years among patients with morbid obesity: the SLEEVEPASS randomized clinical trial. *JAMA* **319**:241–254.
- Scibora LM (2014) Skeletal effects of bariatric surgery: examining bone loss, potential mechanisms and clinical relevance. *Diabetes Obes Metab* **16**:1204–1213.
- Scibora LM, Buchwald H, Petit MA, Hughes J, and Ikramuddin S (2015) Bone strength is preserved following bariatric surgery. *Obes Surg* **25**:263–270.
- Shao Y, Ding R, Xu B, Hua R, Shen Q, He K, and Yao Q (2017) Alterations of gut microbiota after roux-en-Y gastric bypass and sleeve gastrectomy in sprague-dawley rats. *Obes Surg* **27**:295–302.
- Sim BY, Choi HJ, Kim MG, Jeong DG, Lee DG, Yoon JM, Kang DJ, Park S, Ji JG, Joo IH, et al. (2018) Effects of ID-CBT5101 in preventing and alleviating osteoarthritis symptoms in a monosodium iodoacetate-induced rat model. *J Microbiol Biotechnol* **28**:1199–1208.
- Stein EM and Silverberg SJ (2014) Bone loss after bariatric surgery: causes, consequences, and management. *Lancet Diabetes Endocrinol* **2**:165–174.
- Sun MF and Shen YQ (2018) Dysbiosis of gut microbiota and microbial metabolites in Parkinson's Disease. *Ageing Res Rev* **45**:53–61.
- Yan J, Herzog JW, Tsang K, Brennan CA, Bower MA, Garrett WS, Sartor BR, Aliprantis AO, and Charles JF (2016) Gut microbiota induce IGF-1 and promote bone formation and growth. *Proc Natl Acad Sci USA* **113**:E7554–E7563.
- Yang X, Jiang T, Wang Y, and Guo L (2019) The role and mechanism of SIRT1 in resveratrol-regulated osteoblast autophagy in osteoporosis rats. *Sci Rep* **9**:18424–18424xxxx.
- Ying LD, Breuer GA, Hubbard MO, Nadzam GS, Hwa J, and Martin KA (2019) Technical feasibility of a murine model of sleeve gastrectomy with ileal transposition. *Obes Surg* **29**:593–600.
- Yu EW (2014) Bone metabolism after bariatric surgery. *J Bone Miner Res* **29**:1507–1518.
- Zaiss MM, Jones RM, Schett G, and Pacifici R (2019) The gut-bone axis: how bacterial metabolites bridge the distance. *J Clin Invest* **129**:3018–3028.

Address correspondence to: Dr. Jian Du, Department of Endocrinology, The Fourth Affiliated Hospital of China Medical University, No. 4 East Chongshan Rd., Huanggu District, Shenyang, 110032, Liaoning, China. E-mail: dujian035@sina.com